Handling Outliers by Robust M-Estimation in Blind Image Deblurring

Xinxin Zhang, *Student Member, IEEE,* Ronggang Wang, *Member, IEEE,* Da Chen, *Member, IEEE,* Yang Zhao, *Member, IEEE,* Wen Gao, *Fellow, IEEE*

***Abstract*—The major task of traditional motion deblurring methods is to estimate the blur kernel and restore the latent image. In low-light conditions, the pointolite is likely to produce saturated light streaks in captured blurred images. The light streaks are usually double-edged swords — outliers to the deconvolution, but a cue to kernel estimation. In this paper, we propose a novel blind motion deblurring method for blurred images including light streaks. The main idea is to model the non-linear blur caused by outliers as the Huber's M-estimation in blind deconvolution and take the shape of the light streak as a cue to estimate the blur kernel. Specifically, the optimal light streak patch is selected automatically according to the characteristics of light streaks and the blur kernel. This simple yet effective selection strategy solves the problems of false detection of candidate light streaks and optimal light streak in existing methods. Then, the optimal light streak patch is parameterized as a prior and is combined with other regularizers to estimate the blur kernel. Compared with the state-of-the-art kernel estimation methods, the proposed algorithm reduces the influence of outliers on deconvolution and utilizes more information. Thus, the restored image is more accurate. Experimental results on both synthetic and real images demonstrate the high accuracy of our algorithm.**

***Index Terms*—Blind image deblurring, kernel estimation, M-estimator, light streak, outlier.**

I. Introduction

IMAGE motion deblurring is highly demanded in various applications, such as medical analysis, remote sensing, and computer vision. Motion blur is usually caused by the relative motion between the scene and the camera, which is modeled as a convolution process:

$$I = L \otimes k + N, \tag{1}$$

where the symbol $\otimes$ denotes the convolution operator, and I, L, k and N represent the blurred image, sharp latent image, blur kernel, and unknown sensor noise, respectively. The blur kernel is known as the point spread function (PSF) that reflects the trajectory of the camera. The key task of image deblurring is to estimate L from I without specific knowledge of k, and image deblurring can be considered a deconvolution problem. Thus, single image deblurring is a typical ill-posed problem. Hence, smoothness or sparse hypotheses are always required to constrain the latent image and the blur kernel so as to make the problem well-posed.

Due to camera motion in the image capture process, the high-intensity pointolite in low-light conditions, or reflected lights in both low-light and normal illumination conditions often produce several light streaks. When the dynamic range of the scene is higher than that of the camera, the captured intensities are clipped into the dynamic range of a camera, *i.e.*, the maximum or minimum intensity of the dynamic range. Thus, the high-intensity light streaks are prone to be limited by saturation. In this situation, the linear blur model (1) is violated, and severe ringing artifacts are generated even when the blur kernel is known or well-estimated. Hence, the saturated pixels are outliers for the image deblurring problem. Several methods [1]–[5] have been proposed to effectively address the problem in the process of non-blind deconvolution. However, they ignore the removal of adverse effects of outliers in the process of kernel estimation. Moreover, the light streaks usually have strong edges that violate the edge map used in the kernel estimation process. Hence, motion deblurring of images including saturated light streaks is much more challenging. Furthermore, low-light images usually suffer from low contrast and heavy noise, and therefore, a great number of salient-edge-based methods [6]–[9] are likely to fail on low-light images.

Although saturated light streaks create issues in image deblurring, they provide useful information for blur kernel estimation. The most significant is that the light streaks directly reflect the motion trajectory of the camera. Hence, the blur kernel should have a similar shape to the light streaks.

a) Prior art: Motion deblurring has attracted considerable attention and achieved significant progress in recent years. A variety of approaches [8]–[15] have been proposed to solve the motion blur problem. The success of most existing algorithms can be attributed to the use of a wide range of priors. These constraints are used to avoid local minima, dense kernel, and visual artifacts in the restored image. Fergus et al. [11] approximated the full posterior distribution and adopted the ensemble learning method to solve the blur kernel and latent image. Xue and Blu [16], [17] proposed a SURE-based criterion to estimate the blur kernel without relying on edge information. However, these effective methods still cannot effectively handle images that contain outliers.

Another group of methods are the deep neural network (DNN)-based methods [18]–[28]. A number of methods estimate the blur kernel by DNN and get the final latent image

X. Zhang is with the Department of Electronic Engineering, the Chinese University of Hong Kong, Shatin, N.T., Hong Kong (e-mail: xxzhang@ee.cuhk.edu.hk). R. Wang is with the School of Electronic and Computer Engineering, Peking University Shenzhen Graduate School, China (e-mail: rgwang@pkusz.edu.cn). D. Chen is with Qilu University of Technology (Shandong Academy of Sciences), Shandong Artificial Intelligence Institute, China (e-mail: dachen.cn@hotmail.com). Y. Zhao is with the School of Computer and Information, Hefei University of Technology, China (e-mail: zhaoyang@pkusz.edu.cn). W. Gao is with the Department of Computer Science and Technology, Peking University, China (e-mail: wgao@pku.edu.cn).

by non-blind deconvolution. The end-to-end methods learn the latent image from the blurred image by DNN. Li et al. [20] formulated a data-driven discriminative prior to a binary classifier using a deep convolutional neural network. Nimisha et al. [19] proposed a generative adversarial network (GAN)-based unsupervised training deblurring method. However, we have not found any attemps to deal with blurred images including saturated outliers by utilizing DNN. In general, the performance of DNN-based methods is closely associated with the training data. Although most DNN-based methods achieved good performance on synthetic datasets, their performance severely decreased on real-scene images.

In recent years, there have been limited studies using light streaks for motion deblurring. Hua and Low [29] used point light streaks in the blurred image to directly estimate the blur kernel. However, the light streak region was selected manually, which relied on the user's experience and might not be the optimal region. Liu et al. [30] utilized light streak information to refine the shape of the blur kernel. Hu et al. [3], [31] detected the light streak patch automatically and combined the light streak with other image structures to estimate the blur kernel. They set thresholds on maximum image intensity to detect a set of light streaks and discard the patches that contained too many high-intensity pixels. Nevertheless, improper thresholds led to missing detection and false detection.

In terms of deconvolution with outliers, many approaches have been developed in recent years. In practice, many popular methods [32], [33] usually produce severe ringing artifacts even when the blur kernel is known or well-estimated. To suppress ringing artifacts, several non-blind deconvolution methods have been developed. Whyte et al. [1] improved the Richardson-Lucy algorithm to address saturated pixels. Cho et al. [2] employed an expectation-maximization (EM) method to iteratively refine the outlier classification and the latent image. In terms of blind deconvolution, Hu et al. [3], [31] introduced a deconvolution algorithm that combined the advantages of the above two methods to prevent ringing artifacts. Liu et al. [34] detected saturated regions and used non-saturated regions in multi-scale deconvolution to refine the kernel. Pan et al. [4] exploited reliable edges and removed outliers in the intermediate latent images. These methods relied on saturated region detection. It failed in the case of false detection. Dong et al. [5] introduced a new data fidelity term in the kernel estimation to reduce the effect of the outliers. It often failed in the case of daylight blurred images with saturated sunshine or reflect light.

b) Contributions and outline: The major contribution of this paper is to propose an algorithm to eliminate the blur from a single image including saturated light streaks by means of an M-estimator and the light streak information. The light streaks in a blurred image are usually double-edged swords. On one hand, they provide a robust prior to kernel estimation. On the other hand, they are outliers to the deconvolution. In the proposed algorithm, Huber's M-estimator is adopted as the optimizing function to suppress the influence of outliers, and a selected optimal light streak is used to preserve the shape of the blur kernel. This algorithm is robust to outliers in the process of blind deconvolution. Moreover, it makes full use of light streak information to estimate the blur kernel. Compared with the state-of-the-art algorithms, the salient edge extraction method and the optimal light streak selection method in this paper are much simpler, but they achieve comparable results. Note that the proposed method is not specifically designed for low-light images, and thus, can also be applied to normal illumination images.

The rest of the paper is organized as follows. Section II introduces the framework of the proposed algorithm and the theoretical basis of Huber's M-estimator. The iterative estimations of the latent image and blur kernel are then introduced in Section III. Next, we describe the proposed algorithm of kernel estimation in detail in Section IV. Experimental results are discussed in Section V, and Section VI concludes the paper.

II. Iterative framework using robust M-estimator

Currently, the most widely used optimization function in deblurring methods is the least-squares (LS) estimator. However, LS estimators are sensitive to outliers. Hence, we replace the squared residuals by a robust estimator – the Huber's M-estimator that has a greater resistance to outliers. M-estimators are generalizations of the classical maximum likelihood estimates and have been used in denoising [35], [36], image registration [37], [38] and geodesy [39]–[41]. In recent decades, many M-estimators have been proposed. Among them, Huber's M-estimator yields good performance in terms of fine statistical properties and relatively low computational cost.

In this section, a framework of Huber's M-estimator correlation coefficient-based image deblurring is introduced. Fig. 1 shows the framework of the proposed deblurring method. The proposed algorithm is iterated in a coarse-to-fine manner, and the default number of iterations is 5.

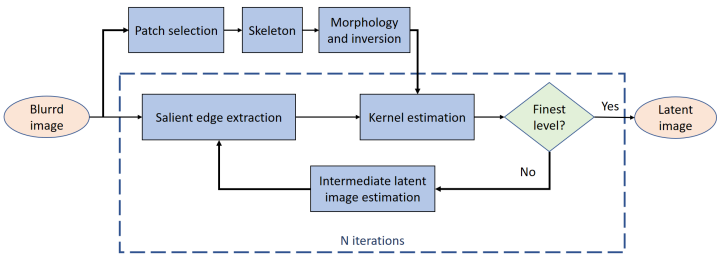

Fig. 1. Framework of the proposed method.

A. Huber's M-estimator

Huber's M-estimator is based on the principles of robust statistics. Huber's function is a parabola around zero and increases linearly at a given level $|x| > t$. Huber's M-estimator attempts to obtain the best of both the least-square estimator in which it is easy to find the minimum, and the absolute deviation estimator that is more robust, which helps restrict the influence of outliers. The ρ-function for Huber's M-estimator is given as follows:

$$\rho(x) = \begin{cases} \dfrac{x^2}{2} & \text{if } |x| < t \\ t(|x| - \dfrac{t}{2}) & \text{if } |x| \geq t \end{cases} \tag{2}$$

where t is a positive tuning threshold. The function $\rho(\cdot)$ is a symmetric positive definite function with a unique minimum at zero and is chosen to increase slower than quadratically.

The influence function $\psi = \frac{d\,\rho(x)}{d\,x}$ describes the sensitivity of the overall estimate on the data with the residual x. For a robust estimator, the influence of any single data point does not introduce any significant error. This influence function is a mixed l_2 and l_1 minimization problem that penalizes the small and high residuals differently. This makes it less sensitive to outliers. The influence function for Huber's M-estimator is given below:

$$\psi(x) = \begin{cases} x & \text{if } |x| < t \\ t\text{sgn}(x) & \text{if } |x| \geq t \end{cases} \tag{3}$$

Using this estimator, an asymptotic efficiency of 95% on the standard normal distribution is obtained with the tuning constant $t = 1.345\sigma$, where σ is the estimated standard deviation of errors. For a blurred image including saturated light streaks, the residuals of saturated light streaks are always larger than t. Thus, the saturated pixels are identified automatically, and the large residuals are substituted by the constant t.

The nature of the ρ-function and the influence function ψ defined in the above equations are shown in Fig. 2 (a) and (b), and those of the least-squares function are shown in Fig. 2 (c) and (d). Fig. 2 (d) shows that the correspondence of the derivation of the least-squares function increases as the residual becomes larger. However, the correspondence of $\psi(x)$-function stops when the residual is larger than a threshold. Hence, Huber's M-estimator is more robust to outliers. From the comparison, we can find the advantage of Huber's M-estimator over the least-squares function.

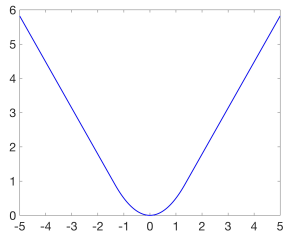

(a) Huber's M-estimator: ρ-function

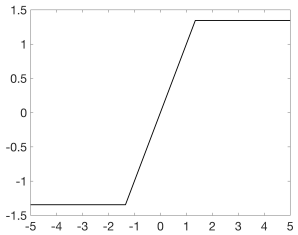

(b) Huber's M-estimator: ψ-function

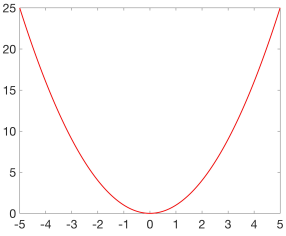

(c) Least-squares function

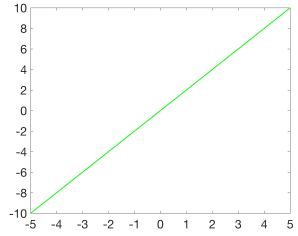

(d) Derivation of the least-squares function

Fig. 2. The diagrams show the comparison of Huber's M-estimator and the least squares function and the corresponding influence functions.

B. Image Deblurring using Huber's M-estimator

For the deblurring problem, we define the residual vector as

$$x = L \otimes k - I. \tag{4}$$

The kernel is estimated by combining the light streak information with other priors, and using Huber's M-estimator as the data fidelity, thus the objective function becomes

$$E_{L,k} = \rho(x) + \eta R_L(L) + \beta R_k(k), \tag{5}$$

where $R_L(L)$ and $R_k(k)$ are the priors on the latent images and the kernel, η and β are the corresponding weights. We utilize the hyper-Laplacian term to constrain the latent image, i.e. $R_L(L) = |\nabla L|^\alpha$, $\nabla L = (\partial_x L, \partial_y L)$. In terms of the kernel prior, we combine the kernel shape and l_2 regularization to regularize the kernel, i.e. $R_k(k) = \beta\|k_0 \circ k\|_2^2$. The symbol $\circ$ denotes the Hadamard product. And k_0 is a 2D binary mask matrix, in which the element is 0 if it belongs to the light streak; otherwise, it is 1. This mask restrains the shape of the kernel.

To solve the ill-posed deblurring problem, we iteratively estimate the latent image L and the blur kernel k. That is to optimize the following objective functions:

$$E_L = \rho(L \otimes k - I) + \eta|\nabla L|^\alpha \tag{6}$$

$$E_k = \rho(L \otimes k - I) + \beta\|k_0 \circ k\|_2^2. \tag{7}$$

The details of optimization and light streak selection are shown in Section III and Section IV.

From function (2) we know that the data fidelity term $\rho(x)$ is a mixed l_2 and l_1 minimization problem. Instead of optimizing the Huber's M-estimator-based objective function directly, a weighted least-squares estimator is used to replace $\rho(x)$ [42], [43]. Define the weight function $w(x) = \frac{\psi(x)}{x}$, hence, different weights are assigned to different points. The nature of the weight function is shown in Fig. 3 (a). We can find that a small weight $w(x_i) = \frac{\psi(x_i)}{x_i}$ is assigned to a large residual so as to prevent the influence of outliers. In the deblurring problem, the saturated light streaks have large residuals, thus the corresponding weights are small. Hence, the influence of light streaks on the deconvolution is waning. In terms of the least squares estimator, the weights are the same for all the points. Hence, the weighted least-squares estimator outperforms the least squares estimator.

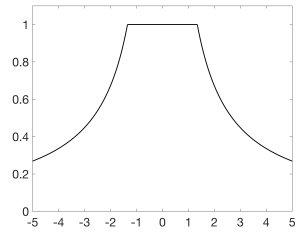

(a) Weight function of Huber's M-estimator

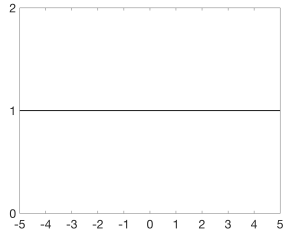

(b) Weight function of the least-squares estimator

Fig. 3. The diagrams show the comparison of the weight functions of Huber's M-estimator and the least-squares estimator.

Fig. 4 shows the comparison of results using the least-squares estimator and Huber's estimator. In terms of the daylight partially saturated blurred image, the light streak is usually caused by reflection. In this comparison, the settings are all the same except for the optimization functions. The severe ringing artifacts and the inaccurate kernel in (b) illustrate that the least-squares estimator is sensitive to the saturated pixels (the reflective area on the refrigerator handle). In (c), the estimated kernel has a very similar shape to that of the light streak. Hence, Huber's estimator is a more appropriate optimization function.

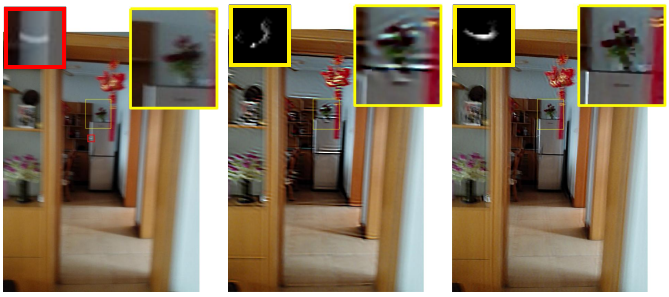

(a) Blurred image (b) Least squares estimator (c) Huber's M-estimator

Fig. 4. (a) is the blurred image, (b) and (c) are the results of using the least squares estimator and Huber's estimator as the optimization function, respectively. In (a), the selected optimal light streak patch is shown at the top-left corner. In (b) and (c), the estimated kernel is shown at the top-left corner.

III. LATENT IMAGE ESTIMATION

As introduced in Section II, the deblurring problem is addressed by iteratively estimating the latent image and the blur kernel. When k is fixed, L is estimated by minimizing the energy function (6). In general, α is set to 0.5 to 0.8 so as to well model the distribution of gradients in natural scenes [44]. In this paper, α is set to 0.6.

The half-quadratic penalty method [45] is used to solve the highly non-convex function. We introduce an auxiliary variable u to substitute ∇L and change (6) to the following optimization problem:

$$E_L = \rho(L \otimes k - I) + \eta|u|^\alpha + \eta_1\|\nabla L - u\|_2^2, \tag{8}$$

where η_1 is a weight, and when it is close to ∞, the solution of (8) converges to that of (6). We solve (8) by iteratively updating u and L. By fixing all the variables except u, Eq (8) is simplified to

$$E_u = \eta|u|^\alpha + \eta_1\|\nabla L - u\|_2^2. \tag{9}$$

The Newton-Paphson method is adopted to find u.

Then, we fix u from the previous iteration, and L can be optimized by minimizing:

$$E_L = \rho(L \otimes k - I) + \eta_1\|\nabla L - u\|_2^2, \tag{10}$$

where the iteratively reweighted least-squares (IRLS) method [46] with the weight function $w(x)$ is utilized to find L [42], [43]. Iterating the above two steps twenty times is sufficient to obtain a satisfactory latent image.

IV. KERNEL ESTIMATION WITH LIGHT STREAKS

Kernel estimation is the most pivotal step in the image deblurring process because a high quality latent image introduced in Section III relies on an accurate blur kernel. In this section, we use the light streak information as a cue to estimate the blur kernel.

The blur kernel can be separated into trajectory (shape) and intensity. A light streak is formed by the movement of a small group of high-intensity pixels and represents the motion trajectory of the camera. Therefore, we can obtain the shape information of the blur kernel from the selected light streaks. The kernel can be estimated by combining the light streak with other regulations.

A. Salient Edge Extraction

Edge information violates kernel estimation when the scale of an object is smaller than that of the blur kernel, while effective salient edges can avoid the delta kernel and obtain an accurate blur kernel. Therefore, we remove tiny edges from ∇L and retain the salient edges ∇S for kernel estimation. The salient edges are extracted as the 95% largest values of gradients, and the 95% threshold is chosen based on numerous experiments. This salient edge selection method has a similar performance to the popular edge extraction method [7], [8], [13], but it is much simpler. The saturated light streaks always violate the edge map because they have very strong boundaries. Whereas, a reliable edge map should only contains the salient edges of objects in a scene. The unreliable salient edge map further leads to an inaccurate blur kernel. However, the proposed method addresses this problem effectively by utilizing M-estimators. As analysis in Section II.B, the saturated light streaks are identified by Huber's M-estimator and are given small weights in the estimation.

B. Light Streaks Selection

In the proposed method, the optimal light streak selection plays a vital role in kernel estimation. However, an image may contain many light streaks, and the selection of the optimal light streak is also a challenging problem. Hua and Low [29] manually selected the light streak, which relied on the users' experience. Hu et al. [3] automatically detected the light streak patch. However, their algorithm is sensitive to the selected light streak, and the false selection leads to unreliable results. Different from the priority of unsaturated light streak in the process of the best patch detection described in [3], the proposed method is robust to both unsaturated and saturated light streaks, and it has been demonstrated in the later analysis and experiments.

Based on the observations, we find that a reliable light streak patch always possesses the following characteristics:

(1) the light streaks may not have to be saturated, as long as their intensities are much higher than those of their neighbors;
(2) there are salient boundaries between light streaks and other areas;
(3) the light streak should be located at the centre of the patch;

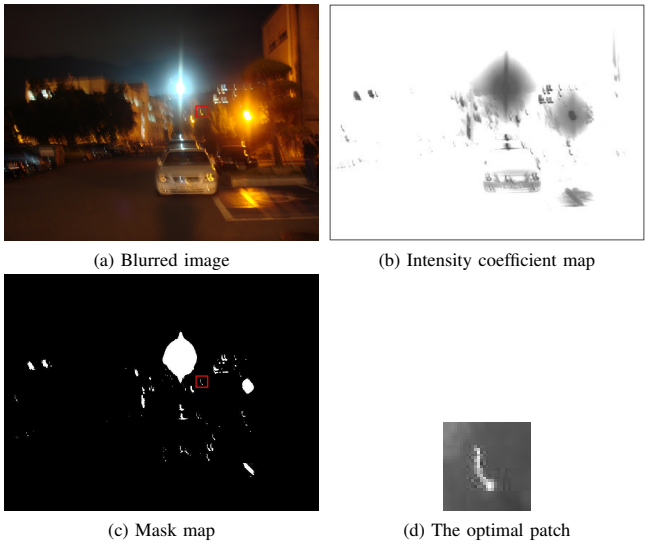

(a) Blurred image (b) Intensity coefficient map

(c) Mask map (d) The optimal patch

Fig. 5. An example of optimal patch selection.

(4) the light streaks should have a sparse distribution; in other words, the candidate light streaks are very thin;
(5) each candidate patch contains one and only one obvious bright light streak;
(6) the shape of the light streak is similar to that of most candidate light streaks.

Fig. 6. The optimal light streak selection. The light streaks in red and cyan rectangles are the selected candidate light streaks. The light streak in the cyan rectangle is the selected optimal one.

First, several candidate light streaks are selected automatically from the input blurred image according to the characteristics (1) to (4). Then the optimal light streak is selected from the candidate light streaks according to the characteristics (5) and (6). An example of optimal light streak selection process is shown in Fig. 5. According to the abovementioned features (1) and (2), we compute the intensity coefficient map of the input image:

$$c = \frac{\max(I)}{I_r + I_g + I_b}, \tag{11}$$

where I is the blurred images, I_r, I_g and I_b indicate R, G and B channels, respectively. The intensity coefficient map is shown in Fig. 5 (b). Then, the pixels of the 3% smallest values of c are set to 1, and the others are set to 0. This mask map is shown in Fig. 5 (c). After that, several patches containing light streaks are selected from this mask map, and the light streak is adjusted to the centre of the patch to satisfy the characteristic of (3). According to the characteristic (4), we compute the sparsity of each patch and choose patches with smaller sparsities. Our strategy is to calculate the ratio between the number of pixels larger than 0.8 and the total number in the patch. The smaller the ratio is, the sparser the patch is. Afterwards, some patches containing a large light source or multiple light streaks are removed. According to characteristics (5) and (6), we compute the SSIM between one patch and the other patches, and the patch with the largest summation of SSIM values is regarded as the optimal patch. The final selected optimal light streak patch is shown in Fig. 5 (d).

The description of the optimal light streak selected from the candidate light streaks is shown in Fig. 6. The light streaks in red and cyan rectangles are the selected candidate light streaks. Because of the limited space, we just show the mask maps of eight typical candidate light streaks for analysis. According to features (1), (2) and (3), a number of patches containing high intensity pixels are selected, which are surrounded by yellow, red and cyan rectangles. By computing the sparsity of each patch according to the characteristic (4), patches in yellow rectangles are excluded from the candidate patches. At last, we choose the patch with the largest summation of SSIM values from all the candidate patches as the optimal light streak patch, which is in the cyan rectangle.

Additionally, note that if there is no detected optimal light streak in the input blurred image, we set the selected patch as an all-ones matrix. This situation often occurs under normal lighting conditions.

C. Kernel Estimation With Shape Prior

We use the optimal light streak to guide the kernel shape and refine the estimation of the kernel. After selecting the optimal light streak patch, the patch is converted to a four-pixel-width binary trajectory by skeletonization and morphology processing. This process is shown in Fig. 7. Then, the binary map is inverted and denoted by k_0. Thus, the element in k_0 equals 0 if its corresponding pixel belongs to the trajectory, and equals 1 otherwise.

We then combine the Gaussian regularizer with the shape prior to restraining the kernel shape and guaranteeing the continuity of the kernel. The salient edges ∇S extracted from the intermediate latent image obtained in the preceding step described in Section III is used to estimate the kernel by minimizing the energy function:

$$\begin{aligned} &E_k = \rho(\nabla S \otimes k - \nabla I) + \beta \|k_0 \circ k\|_2^2 \\ &s.t.\ k(i) \geq 0, \quad \sum_i k(i) = 1. \end{aligned} \tag{12}$$

The blur kernel is obtained by optimizing the convex function (12). Under normal lighting conditions, k_0 is an all-ones matrix. In this case, (12) becomes an objective function which has been used in many state-of-the-art blur kernel estimation

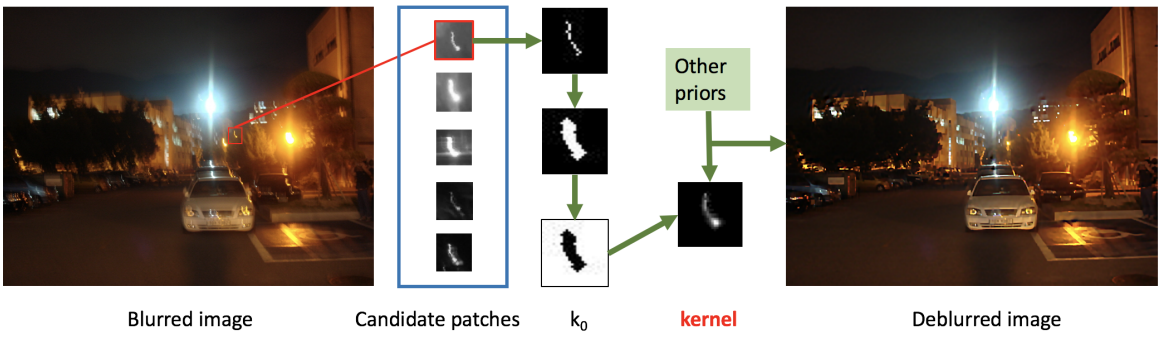

Fig. 7. The pipeline of kernel estimation.

methods. Hence, (12) shows the generality of the proposed algorithm.

Fig. 8 shows the comparison of the results with and without the light streak shape prior in kernel estimation. We can see that the kernel in (c) has a similar shape to the light streak; however, the kernel in (b) is a delta kernel. The deblurred image in (c) is much clearer than that in (b). The comparison demonstrates that the shape prior plays a significant role in kernel estimation.

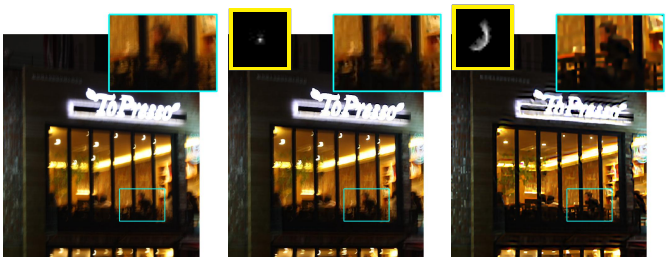

(a) Blurred image (b) Without the shape prior (c) With the shape prior

Fig. 8. The comparison of the results with and without the light streak shape prior. The estimated kernel is shown at the top-left corner.

Fig. 9 illustrates different deblurred results with different light streaks. We find that different light streaks lead to different deblurred images. The automatic selected light streak patch is patch 1. We select three other patches manually and estimate the kernels and the deblurred results. The four patches have the same size to avoid the influence of the kernel size. From the deblurred results shown in Fig. 9, it can be found that the deblurred result with the automatically selected patch is of the highest quality, and the shape of the estimated kernel is the most similar to that of the light streaks. The results with patch 2 and patch 4 are also good enough for practical applications. Hence, the proposed method is robust to light streak patch selection; that is, more than one light streak patch for the proposed kernel estimation method may be appropriate. In terms of patch 3, the thick light streak leads to severe ringing artifacts in the deblurred result. However, this condition is easily excluded by our light streak selection strategy.

V. Experimental Results

A. Experimental setting

Image deblurring benefits a number of real-world applications. In this section, to verify our algorithm, extensive experiments are performed on both synthetic datasets and real images with the proposed method.

We compare our method with several existing state-of-the-art deblurring methods. In terms of the comparison on low-light images, we mainly consider two low-light deblurring methods, including a blind deblurring method that handles saturated pixels and non-Gaussian noise [4], and a low-light image deblurring method that depends on the light streak [3]. Furthermore, we also consider five general deblurring methods that are not designed specifically for light streak images, including a method that relies on salient structures for kernel estimation [47], a kernel refinement method via iterative support detection [7], a deblurring method using L_0 sparse expression [9], a blind deconvolution method using a normalized sparsity regularization term, which gives the lowest cost for the true sharp image [48], and a text deblurring method using L_0 regularized intensity and gradient prior [6]. In addition, we consider five DNN-based methods: a blind image deblurring method based on a data-driven discriminative prior [20], a blind image deblurring method that utilizes a data-driven approach to learn effective data fitting functions from a large set of motion-blurred images with the associated ground truth blur kernels [23], a method learns a deep convolutional neural network for extracting sharp edges from blurred images [18], a method that proposes a Scale-recurrent Network (SRN-DeblurNet) for multi-scale image deblurring [28], and a method that incorporates gyroscope measurements into a convolutional neural network [27].

To be fair, not only do we run the algorithms under their default configuration, but we also check whether tuning some of their parameters (e.g., number of iterations, kernel size) results in significant accuracy improvements–and if so, show these results instead. In terms of DNN-based methods, we utilize their pre-trained networks. Since the DNN-based methods rely on the training data, their performance may improve if they are re-trained by images including saturated light streaks.

In this section, we illustrate the effectiveness of the proposed algorithm from three aspects. First, we test the accuracy of light streak selection on a publicly available dataset [3]. Second, our algorithm is performed on two synthetic datasets, including a dataset consists of low-light images with saturated light streaks [3], and a dataset consists of day-light motion blurred images without saturated regions [49]. Third, we test

(a) (b) (c) (d) (e)

Fig. 9. The diagrams show the deblurred results with four different light streak patches. (a) is the blurred image. The four patches are selected manually, and they have the same size. They are marked with red rectangles and are numbered from 1 to 4. (b), (c), (d), and (e) are the deblurred results that correspond to patches 1, 2, 3, and 4, respectively. The estimated blur kernels are shown at the top-left corner in images (b), (c), (d), (e).

our algorithm on several real images taken from some modern works or taken by our own smartphone cameras. In addition, we show the comparing results of our algorithm and the state-of-the-art algorithms.

B. Accuracy of light streak selection

In general, accurate light streak selection improves the accuracy of kernel estimation. We tested the accuracy of the light streak selection method on Hu's dataset [3]. This synthetic dataset of uniform blurred images is created for quantitative evaluation. They captured 11 clear low-light images and blurred each image by 14 different blur kernels firstly, and then added Gaussian noise with 1 percent variance. The whole set consists of 154 synthetic blurred images. We apply our light streak selection method to all images and examine the accuracy of the detected kernel shapes visually. In this experiment, we set the kernels as 35 $\times$ 35-pixel patches by default. From the analysis of Section IV-B and Fig. 9, we know our method has a great tolerance to the selected light streak. So we judge the selection visually. As long as the shape of the extracted skeleton from the selected light streak is the same as that of the ground truth kernel, we consider the light streak selection is correct. We find that our method is successful in 146 images; thus, we achieve an accuracy of 95%. Fig. 10 shows some optimal light streak selection results of our method in some examples. The selected patches match the existing described in Section IV-B. Moreover, their shapes are the same as those of the ground truth kernels.

C. Objective evaluation on synthetic dataset

In terms of low light images with light streaks, the proposed algorithm handles saturated pixels in deconvolution effectively and take the light streak as a cue to estimate kernel. Even though for daytime images without light streaks, the proposed algorithm achieves high-quality performance. In this part, we run our algorithm on two publicly available datasets [3] and [49].

First, we test our deblurring method on the low-light image dataset [3] and compare it with ten deblurring approaches [3], [4], [6]–[9], [18], [23], [47], [48]. Each image in the dataset contains several saturated light streaks. We compute the average kernel similarity (KS) [50] of each estimated kernel, and the results are shown in Tab. I. The kernel similarities of methods [3], [7]–[9], [48] come from [3]. The comparison results of one example from this dataset are shown in Fig. 11. From the results, we find that [7]–[9], [47], [48] obtain delta kernels. The kernel similarities of [3], [4] are close to that of ours, but the restored latent images of [4] suffers from severe ringing artifacts around the saturated regions. And our result illustrates clearer details than that of [3].

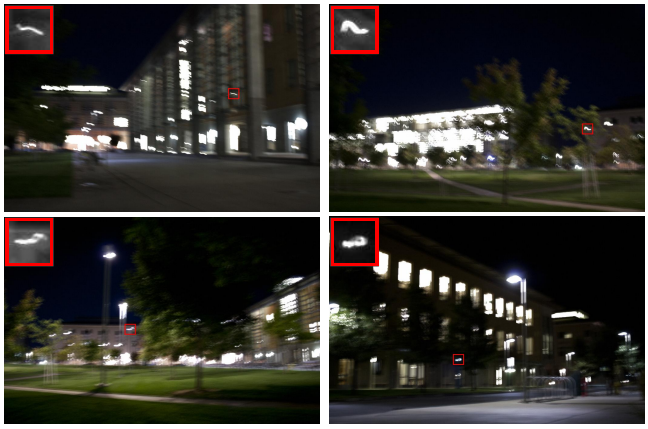

Fig. 10. The diagrams show several examples of our optimal light streak selection results on Hu's dataset [31].

To test the generality of the proposed algorithm, we run our algorithm on a publicly available dataset [49]. It contains 40 sharp images of various scenes, each blurred synthetically with two different kernels and added Gaussian noise of three different levels (σ = 0, 0.01, 0.02). These images contain different numbers of structural edges. Thus, various levels of deblurring difficulties exist for the methods under testing, especially those that rely on salient edge selection. Because most state-of-the-art methods do not handle noisy images specifically, we only use the images with no additional noise for testing. Hence, in our experiment, the number of test blurred images is 80 in total. For the objective evaluation, we adopt the no-reference quality assessment method introduced

TABLE I
THE KERNEL SIMILARITIES OF DIFFERENT METHODS PERFORMED ON THE DATASET [3]

	[3]	[8]	[7]	[9]	[6]	[47]	[48]	[4]	[23]	[18]	**Our**
KS	0.7069	0.5323	0.5185	0.5312	0.5419	0.5345	0.5449	0.7346	0.5295	0.4731	**0.7965**

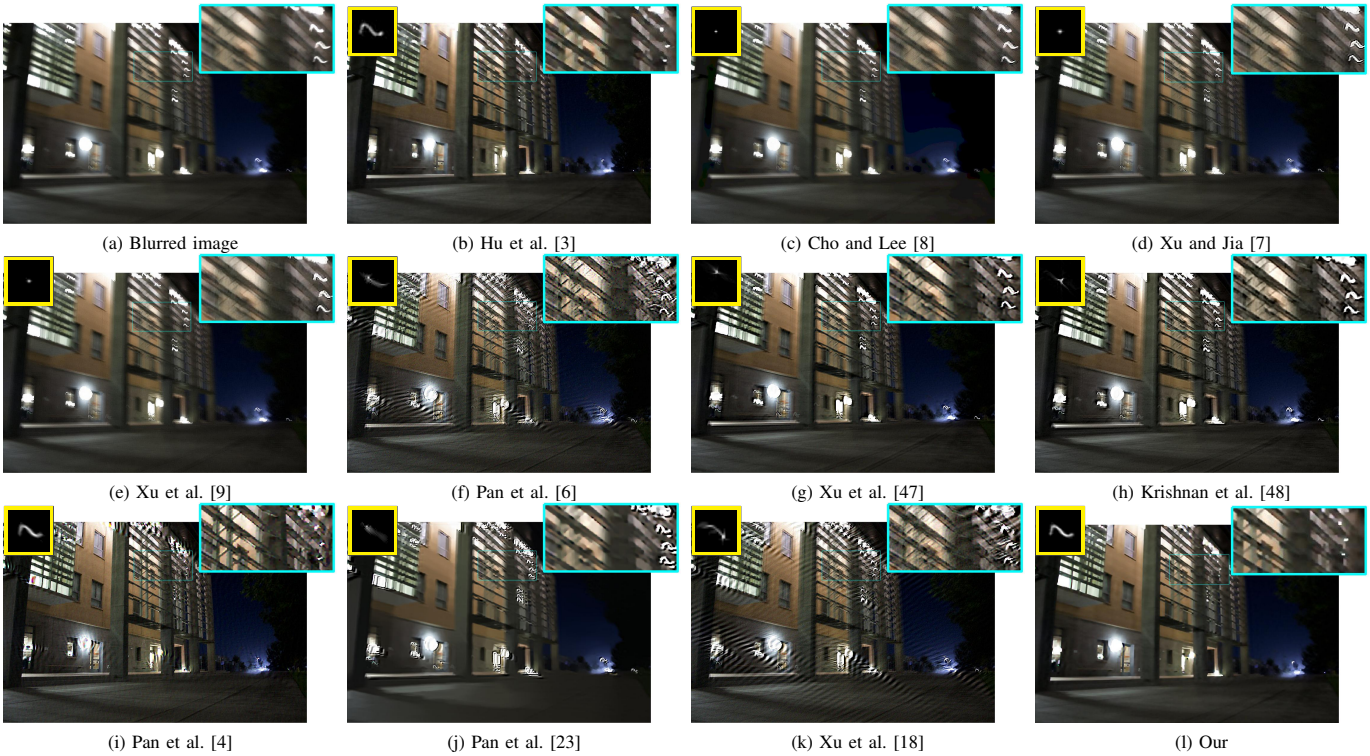

(a) Blurred image (b) Hu et al. [3] (c) Cho and Lee [8] (d) Xu and Jia [7]

(e) Xu et al. [9] (f) Pan et al. [6] (g) Xu et al. [47] (h) Krishnan et al. [48]

(i) Pan et al. [4] (j) Pan et al. [23] (k) Xu et al. [18] (l) Our

Fig. 11. Comparison with state-of-the-art methods on a synthetic example from the dataset of [3]. The kernel similarities of restored images (b)-(l) are 0.8181, 0.3204, 0.3503, 0.3530, 0.6333, 0.5467, 0.4932, 0.8456, 0.5030, 0.3913 and 0.8663, respectively.

in [49] to quantitatively compare our scores against [4], [6], [7], [9], [18], [23], [28], [47], [48] and [27]. Since the method [3] relies heavily on the light streak, it fails on images without the light streak. Hence, we do not compare this method on this dataset.

When adopting the quality evaluation method, all the scores are negative values, and a larger score value means higher quality. For example, the scores of image A and image B are -6 and -8, respectively, which means A has higher quality than B. The average quality scores of different methods are illustrated in Tab. II. We can see that the proposed method performs the best.

Fig. 12 provides one example from the test dataset. Because of the limited space, we only show the best 10 results. The restored images of [27] always suffer from severe ringing artifacts. As shown, the results with other methods, contain various levels of visual artifacts, while the results of [4] and our method are the clearest with richer details and fewer artifacts. Moreover, our result gets the highest score.

D. Subjective evaluation on real images

To demonstrate the practicality of the proposed algorithm, we test our algorithm on several real images and compare it with other competitive methods. These images in this dataset are all blurred images captured by camera phones or taken from other works [1], [2], [4]. The blur is mainly caused by camera shake. Some images are taken under low-light conditions with lamplight, and some images are taken under daylight conditions. Light streaks appear on these images.

Three examples shown in Fig. 13, Fig. 14 and Fig. 15 illustrate that our method outperforms the other comparative state-of-the-art methods. In each image, the estimated kernel is shown at the top-left corner. However, we cannot obtain the estimated blur kernels of [28], so we do not show them in the figures. In Fig. 13, only [4] and [23] obtain comparable restoration results with ours, but there are ringing artifacts around the saturated areas. In Fig. 14, the shape of the blur kernels estimated by these methods except [6], [23], [4] and ours are unreliable. The zoom-in patches located at the top-right corners show that only the results of [4], [28] and our method are clear enough to see the man's appearance. However, [4] suffers from more heavy noise and ringing artifacts than those of ours. There are extra artifacts are produced in several areas (the top-left corner and the bottom-right corner) of output of the [28]. In terms of Fig. 15, all images contain light streaks, which are the lamplights, sunshine or reflected light. We find

TABLE II
QUANTITATIVE COMPARISONS WITH 10 STATE-OF-THE-ART DEBLURRING METHODS ON THE DATASET [49]

	[7]	[9]	[6]	[47]	[48]	[4]	[28]	[23]	[18]	[27]	**Our**
Score 1	-9.58	-9.27	-9.62	-10.40	-11.76	-8.45	-11.13	-10.16	-9.79	-12.90	**-8.03**
Score 2	-9.03	-8.98	-8.64	-9.64	-9.80	-7.87	-10.14	-9.21	-8.20	-11.03	**-7.51**

(1) The row "Score 1" shows the average scores of results from images blurred with kernel 1. (2) The row "Score 2" shows the average scores of results from images blurred with kernel 2. (3) A larger score value means higher quality. (4) Bold values indicate the best results.

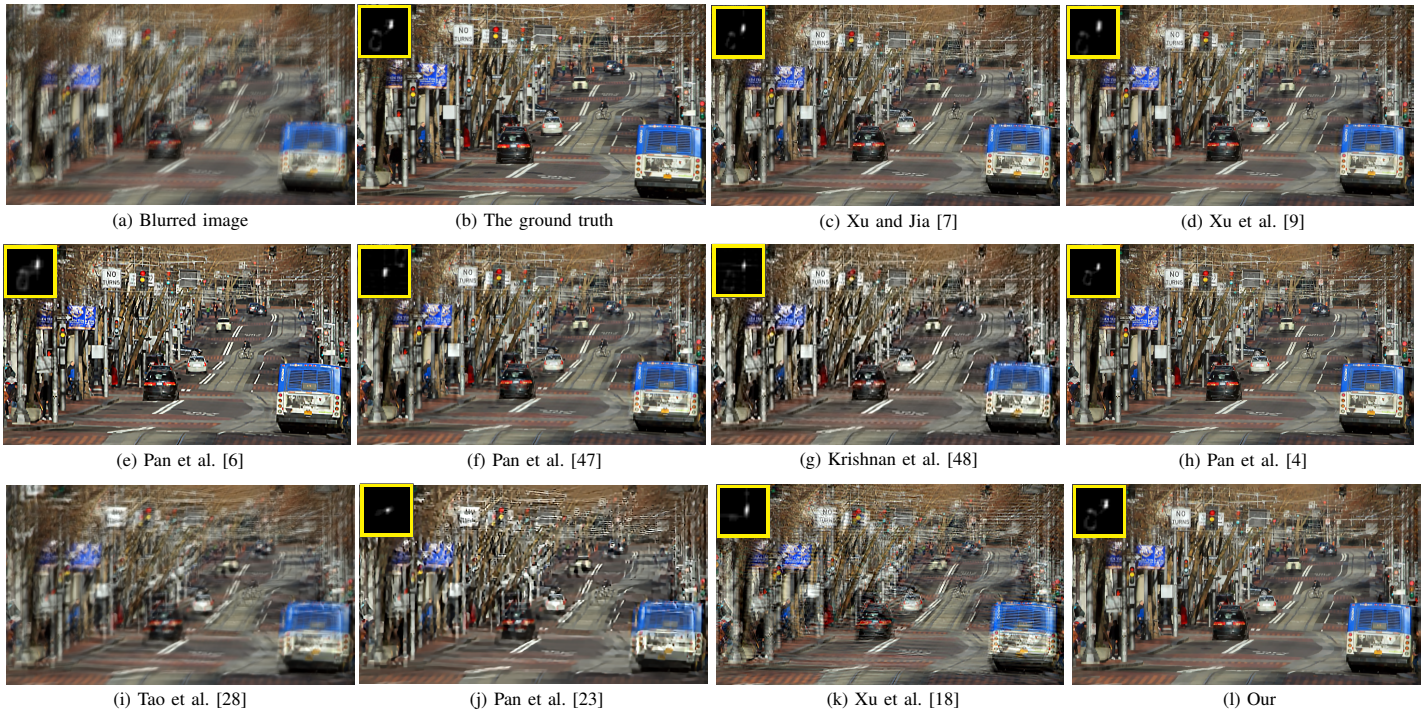

(a) Blurred image (b) The ground truth (c) Xu and Jia [7] (d) Xu et al. [9]

(e) Pan et al. [6] (f) Pan et al. [47] (g) Krishnan et al. [48] (h) Pan et al. [4]

(i) Tao et al. [28] (j) Pan et al. [23] (k) Xu et al. [18] (l) Our

Fig. 12. Comparison with state-of-the-art methods on a synthetic example from the dataset of [49]. The quality scores of restored images (c)-(l) are -10.634, -10.266, -10.235, -10.724, -10.821, -9.436 -13.463, -13.353, -12.632 and -9.231, respectively. Since we cannot obtain the estimated blur kernel of [28], we do not show it in the figure.

that the traditional deblurring methods [6], [7], [9], [47], [48] obtain restoration results with severe ringing artifacts or generate delta blur kernels. The DNN-based methods [18], [23], [27], [28] also have the same problems when we use their pre-trained networks. Hence, we only compare with the methods [3] and [4], which are designed specifically for saturated outliers. From Fig. 15, we can find severe ringing artifacts in all the results of [4] except the result in fourth row, and some results of [3] (the third and the fourth rows).

From examples shown above, we can find that this method is effective for low-light images with saturated light streaks or images without light streaks. For daylight images, the shape of the light streak can guide the kernel shape to generate an accurate result. Fig. 4 and the fifth row in Fig. 15 show two challenging examples of daylight brightness blurred images.

The proposed algorithm is effective and robust; however, it fails in some cases. It fails when the blur is non-uniform or extremely large (the kernel size is larger than the 1/4 of the image size). Another case is that in which some streaks in the blurred image disturb the optimal light streak patch selection. The incorrect light streak leads to an inaccurate kernel.

VI. DISCUSSION AND CONCLUSION

In this work, we proposed a novel blind motion deblurring method to handle outliers in blurred images by optimizing a robust M-estimator. Saturated light streaks and pointolite in the low-light images cause a serious problem for blind deconvolution because they violate the assumption of linear convolution in the blurring process. The M-estimator effectively handles the saturated pixels so as to suppress the ringing artifacts. Additionally, we use light streak information to guide kernel estimation. Specifically, we present a simple yet effective method to select the optimal light streak patch according to the properties of light streaks and the blur kernel. Then, the light streak is used as a cue to estimate the blur kernel so that the blur kernel and the light streak have a similar shape. Compared with other kernel estimation methods, the proposed method utilizes more information, and the kernel is more accurate. Experimental results show that our algorithm not only has a good performance on synthetic images but is also useful in practice.

ACKNOWLEDGEMENT

The authors would like to thank the anonymous reviewers for their helpful suggestions and constructive comments,

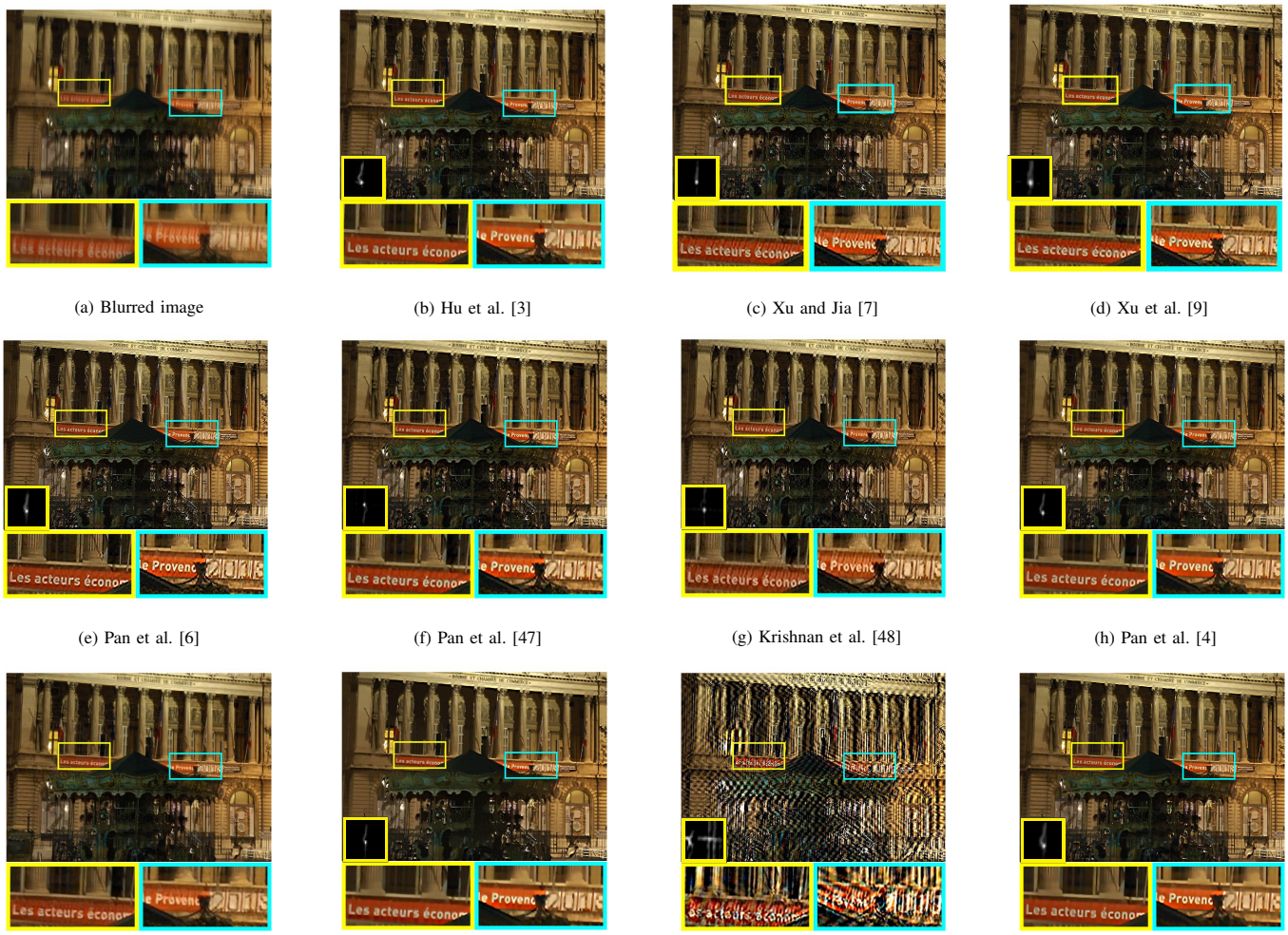

(a) Blurred image (b) Hu et al. [3] (c) Xu and Jia [7] (d) Xu et al. [9]

(e) Pan et al. [6] (f) Pan et al. [47] (g) Krishnan et al. [48] (h) Pan et al. [4]

(i) Tao et al. [28] (j) Pan et al. [23] (k) Xu et al. [18] (l) Our

Fig. 13. Comparison with state-of-the-art methods on a real image.

which have improved the quality of this paper.

REFERENCES

[1] O. Whyte, J. Sivic, and A. Zisserman, "Deblurring shaken and partially saturated images," *International journal of computer vision*, vol. 110, no. 2, pp. 185–201, 2014.

[2] S. Cho, J. Wang, and S. Lee, "Handling outliers in non-blind image deconvolution," in *Computer Vision (ICCV), 2011 IEEE International Conference on*. IEEE, 2011, pp. 495–502.

[3] Z. Hu, S. Cho, J. Wang, and M. Yang, "Deblurring low-light images with light streaks," *IEEE Transactions on Pattern Analysis and Machine Intelligence*, vol. 40, no. 10, pp. 2329–2341, 2018.

[4] J. Pan, Z. Lin, Z. Su, and M.-H. Yang, "Robust kernel estimation with outliers handling for image deblurring," in *Proceedings of the IEEE Conference on Computer Vision and Pattern Recognition*, 2016, pp. 2800–2808.

[5] J. Dong, J. Pan, Z. Su, and M.-H. Yang, "Blind image deblurring with outlier handling," in *Proceedings of the IEEE International Conference on Computer Vision*, 2017, pp. 2478–2486.

[6] J. Pan, Z. Hu, Z. Su, and M.-H. Yang, "Deblurring text images via l0-regularized intensity and gradient prior," in *Proceedings of the IEEE Conference on Computer Vision and Pattern Recognition*, 2014, pp. 2901–2908.

[7] L. Xu and J. Jia, "Two-phase kernel estimation for robust motion deblurring," in *European conference on computer vision*. Springer, 2010, pp. 157–170.

[8] S. Cho and S. Lee, "Fast motion deblurring," in *ACM Transactions on graphics (TOG)*, vol. 28, no. 5. ACM, 2009, p. 145.

[9] L. Xu, S. Zheng, and J. Jia, "Unnatural l0 sparse representation for natural image deblurring," in *Proceedings of the IEEE conference on computer vision and pattern recognition*, 2013, pp. 1107–1114.

[10] X. Yu, F. Xu, S. Zhang, and L. Zhang, "Efficient patch-wise non-uniform deblurring for a single image," *IEEE Transactions on Multimedia*, vol. 16, no. 6, pp. 1510–1524, 2014.

[11] R. Fergus, B. Singh, A. Hertzmann, S. T. Roweis, and W. T. Freeman, "Removing camera shake from a single photograph," in *ACM transactions on graphics (TOG)*, vol. 25, no. 3. ACM, 2006, pp. 787–794.

[12] Q. Shan, J. Jia, and A. Agarwala, "High-quality motion deblurring from a single image," in *ACM transactions on graphics (TOG)*, vol. 27, no. 3. ACM, 2008, p. 73.

[13] X. Zhang, R. Wang, Y. Tian, W. Wang, and W. Gao, "Image deblurring using robust sparsity priors," in *Image Processing (ICIP), 2015 IEEE International Conference on*. IEEE, 2015, pp. 138–142.

[14] Y. Han and J. Kan, "Blind color-image deblurring based on color image gradients," *Signal Processing*, vol. 155, pp. 14–24, 2019.

[15] D. Gong, R. Li, Y. Zhu, H. Li, J. Sun, and Y. Zhang, "Blind image deblurring by promoting group sparsity," *Neurocomputing*, vol. 310, pp. 190–200, 2018.

[16] F. Xue and T. Blu, "A novel sure-based criterion for parametric psf estimation," *IEEE Transactions on Image Processing*, vol. 24, no. 2, pp. 595–607, 2015.

[17] F. Xue, F. Luisier, and T. Blu, "Multi-wiener sure-let deconvolution," *IEEE Transactions on Image Processing*, vol. 22, no. 5, pp. 1954–1968, 2013.

[18] X. Xu, J. Pan, Y.-J. Zhang, and M.-H. Yang, "Motion blur kernel estimation via deep learning," *IEEE Transactions on Image Processing*, vol. 27, no. 1, pp. 194–205, 2018.

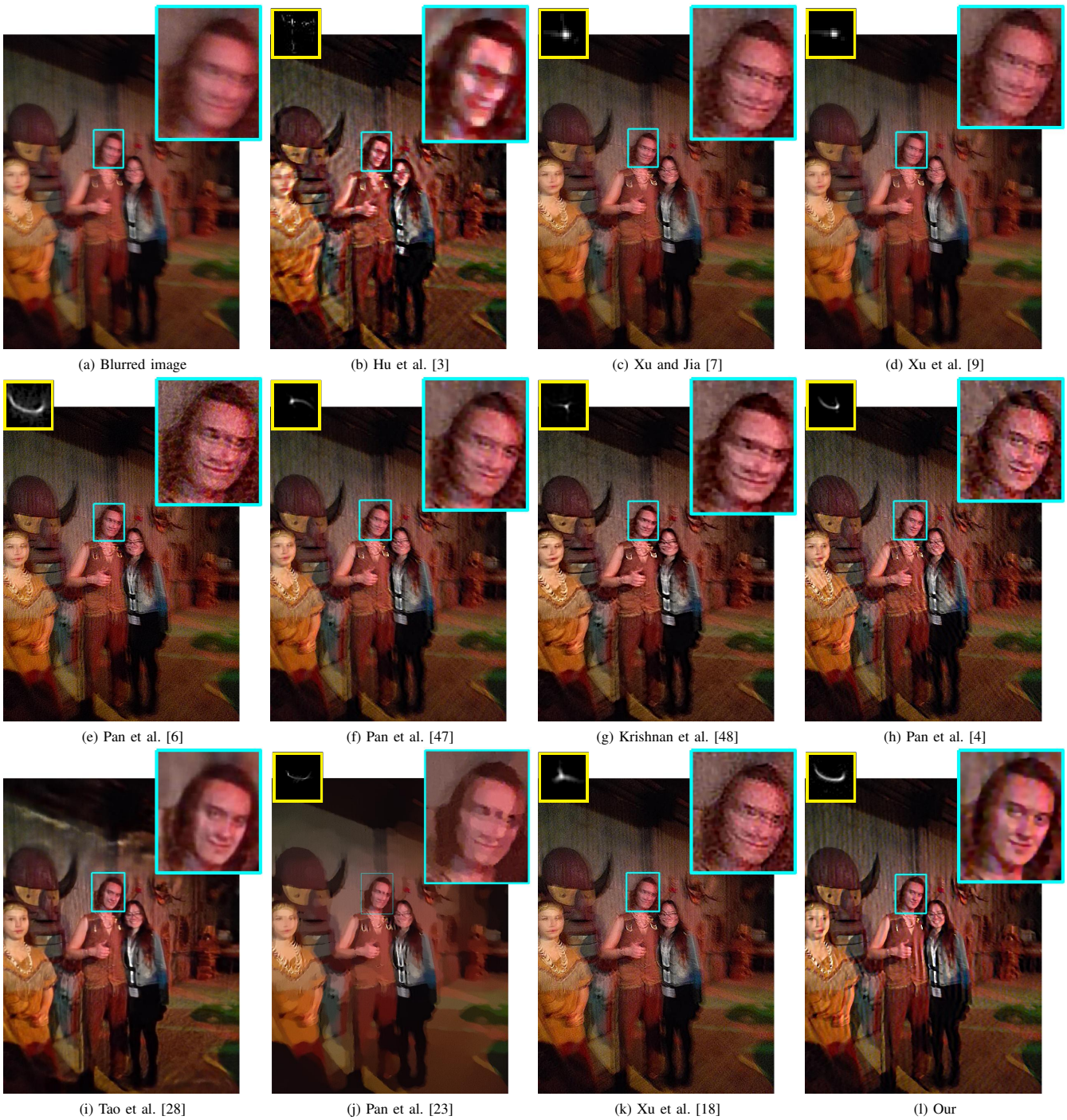

(a) Blurred image (b) Hu et al. [3] (c) Xu and Jia [7] (d) Xu et al. [9]

(e) Pan et al. [6] (f) Pan et al. [47] (g) Krishnan et al. [48] (h) Pan et al. [4]

(i) Tao et al. [28] (j) Pan et al. [23] (k) Xu et al. [18] (l) Our

Fig. 14. Comparison with state-of-the-art methods on a real image captured by a camera phone.

[19] T. Madam Nimisha, K. Sunil, and A. Rajagopalan, "Unsupervised class-specific deblurring," in *Proceedings of the European Conference on Computer Vision (ECCV)*, 2018, pp. 353–369.

[20] L. Li, J. Pan, W.-S. Lai, C. Gao, N. Sang, and M.-H. Yang, "Blind image deblurring via deep discriminative priors," *International Journal of Computer Vision*, pp. 1–19, 2019.

[21] J. Pan, W. Ren, Z. Hu, and M.-H. Yang, "Learning to deblur images with exemplars," *IEEE transactions on pattern analysis and machine intelligence*, vol. 41, no. 6, pp. 1412–1425, 2018.

[22] J. Dong, J. Pan, D. Sun, Z. Su, and M.-H. Yang, "Learning data terms for non-blind deblurring," in *Proceedings of the European Conference on Computer Vision (ECCV)*, 2018, pp. 748–763.

[23] J. Pan, J. Dong, Y.-W. Tai, Z. Su, and M.-H. Yang, "Learning discriminative data fitting functions for blind image deblurring," in *Proceedings of the IEEE International Conference on Computer Vision*, 2017, pp. 1068–1076.

[24] H. Sim and M. Kim, "A deep motion deblurring network based on per-pixel adaptive kernels with residual down-up and up-down modules," in *Proceedings of the IEEE Conference on Computer Vision and Pattern Recognition Workshops*, 2019, pp. 0–0.

[25] X. Wang, K. C. Chan, K. Yu, C. Dong, and C. Change Loy, "Edvr: Video restoration with enhanced deformable convolutional networks," in *Proceedings of the IEEE Conference on Computer Vision and Pattern Recognition Workshops*, 2019, pp. 0–0.

[26] O. Kupyn, V. Budzan, M. Mykhailych, D. Mishkin, and J. Matas, "Deblurgan: Blind motion deblurring using conditional adversarial networks," in *Proceedings of the IEEE Conference on Computer Vision and Pattern Recognition*, 2018, pp. 8183–8192.

[27] J. Mustaniemi, J. Kannala, S. Särkkä, J. Matas, and J. Heikkila, "Gyroscope-aided motion deblurring with deep networks," in *2019 IEEE*

Winter Conference on Applications of Computer Vision (WACV). IEEE, 2019, pp. 1914–1922.
[28] X. Tao, H. Gao, X. Shen, J. Wang, and J. Jia, "Scale-recurrent network for deep image deblurring," in *Proceedings of the IEEE Conference on Computer Vision and Pattern Recognition*, 2018, pp. 8174–8182.
[29] B.-S. Hua and K.-L. Low, "Interactive motion deblurring using light streaks," in *Image Processing (ICIP), 2011 18th IEEE International Conference on*. IEEE, 2011, pp. 1553–1556.
[30] X. Liu, B. Liu, M. Liu, W. Wang, and Z. Yu, "Image deblurring based on light streak shape," *Journal of Electronic Imaging*, vol. 25, no. 2, p. 023016, 2016.
[31] Z. Hu, S. Cho, J. Wang, and M.-H. Yang, "Deblurring low-light images with light streaks," in *Proceedings of the IEEE Conference on Computer Vision and Pattern Recognition*, 2014, pp. 3382–3389.
[32] D. Fish, A. Brinicombe, E. Pike, and J. Walker, "Blind deconvolution by means of the richardson–lucy algorithm," *JOSA A*, vol. 12, no. 1, pp. 58–65, 1995.
[33] E. Sekko, G. Thomas, and A. Boukrouche, "A deconvolution technique using optimal wiener filtering and regularization," *Signal processing*, vol. 72, no. 1, pp. 23–32, 1999.
[34] H. Liu, X. Sun, L. Fang, and F. Wu, "Deblurring saturated night image with function-form kernel," *IEEE Transactions on Image Processing*, vol. 24, no. 11, pp. 4637–4650, 2015.
[35] T. Rabie, "Robust estimation approach for blind denoising," *IEEE Transactions on Image Processing*, vol. 14, no. 11, pp. 1755–1765, 2005.
[36] D. J. Peter, V. Govindan, and A. T. Mathew, "Nonlocal-means image denoising technique using robust m-estimator," *Journal of computer science and technology*, vol. 25, no. 3, pp. 623–631, 2010.
[37] K. Arya, P. Gupta, P. K. Kalra, and P. Mitra, "Image registration using robust m-estimators," *Pattern Recognition Letters*, vol. 28, no. 15, pp. 1957–1968, 2007.
[38] M. M. Fouad, R. M. Dansereau, and A. D. Whitehead, "Image registration under illumination variations using region-based confidence weighted m-estimators," *IEEE transactions on image processing*, vol. 21, no. 3, pp. 1046–1060, 2012.
[39] J. Awange, , and F. Aduol, "An evaluation of some robust estimation techniques in the estimation of geodetic parameters," *Survey Review*, vol. 35, no. 273, pp. 146–162, 1999.
[40] X. Peiliang, "On robust estimation with correlated observations," *Bulletin géodésique*, vol. 63, no. 3, pp. 237–252, 1989.
[41] H. Fuchs, "Contribution to the adjustment by minimizing the sum of absolute residuals," *Manuscripta Geodaetica*, vol. 7, no. 3, pp. 151–207, 1982.
[42] J. Fox *et al.*, "Robust regression," *An R and S-Plus companion to applied regression*, p. 91, 2002.
[43] A. Ruckstuhl, "Robust fitting of parametric models based on m-estimation," *Lecture notes*, 2014.
[44] D. Krishnan and R. Fergus, "Fast image deconvolution using hyper-laplacian priors," in *Advances in Neural Information Processing Systems*, 2009, pp. 1033–1041.
[45] D. Geman and C. Yang, "Nonlinear image recovery with half-quadratic regularization," *IEEE Transactions on Image Processing*, vol. 4, no. 7, pp. 932–946, 1995.
[46] P. W. Holland and R. E. Welsch, "Robust regression using iteratively reweighted least-squares," *Communications in Statistics-theory and Methods*, vol. 6, no. 9, pp. 813–827, 1977.
[47] J. Pan, R. Liu, Z. Su, and X. Gu, "Kernel estimation from salient structure for robust motion deblurring," *Signal Processing: Image Communication*, vol. 28, no. 9, pp. 1156–1170, 2013.
[48] D. Krishnan, T. Tay, and R. Fergus, "Blind deconvolution using a normalized sparsity measure," in *CVPR 2011*. IEEE, 2011, pp. 233–240.
[49] Y. Liu, J. Wang, and Cho, "A no-reference metric for evaluating the quality of motion deblurring," *ACM Trans. Graph*, vol. 32, no. 6, pp. 175–186, 2013.
[50] Z. Hu and M.-H. Yang, "Good regions to deblur," in *European conference on computer vision*. Springer, 2012, pp. 59–72.

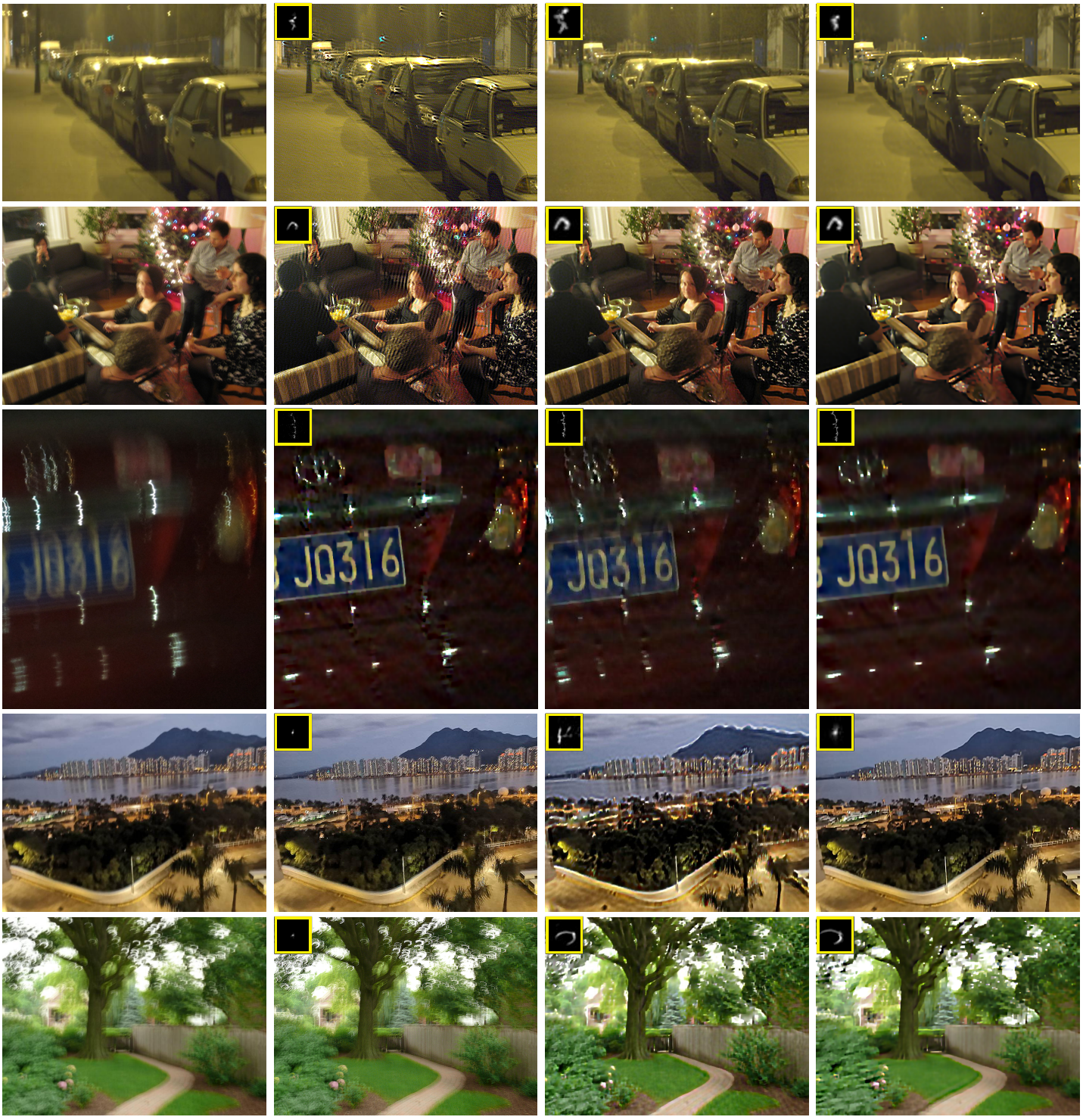

(a) Blurred image (b) Pan et al. [4] (c) Hu et al. [3] (d) Our

Fig. 15. Comparison with two state-of-the-art methods on several real images.